

This work was written as part of one of the author's official duties as an Employee of the United States Government and is therefore a work of the United States Government. In accordance with 17 U.S.C. 105, no copyright protection is available for such works under U.S. Law. Access to this work was provided by the University of Maryland, Baltimore County (UMBC) ScholarWorks@UMBC digital repository on the Maryland Shared Open Access (MD-SOAR) platform.

Please provide feedback

Please support the ScholarWorks@UMBC repository by emailing scholarworks-group@umbc.edu and telling us what having access to this work means to you and why it's important to you. Thank you.

Supporting Information

Ultrafast Carrier Dynamics of Monolayer WS₂ via Broad-Band Time-Resolved Terahertz Spectroscopy

Jon K. Gustafson^{*,1}, Paul D. Cunningham², Kathleen M. McCreary², Berend T. Jonker², and L. Michael Hayden^{*,1}

¹Department of Physics, UMBC, 1000 Hilltop Circle Baltimore, MD 21250, United States

²U.S. Naval Research Laboratory, Washington, D.C. 20375, United States

**Corresponding authors: jgus1@umbc.edu, hayden@umbc.edu*

Terahertz Waveform and Spectra

In Figure S1a, we display the measured electric field of a terahertz pulse as a function of time. In order to resolve the electric field of the terahertz waveform, we employed electro-optic sampling¹ in a 300 μm thick GaP crystal. The resulting amplitude and phase spectra are shown in Figure S1b. Continuous bandwidth from 0.5 to 8 THz was typical of our setup.

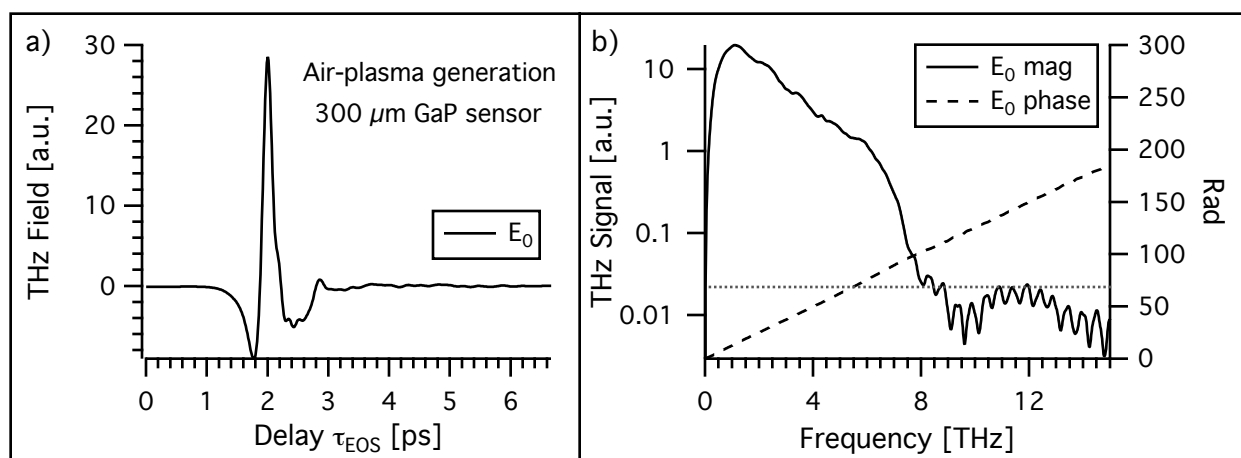


Figure S1. (a) Time-domain trace of a terahertz waveform generated via air-plasma and detected via electro-optic sampling (EOS). (b) Fourier transform of the time-domain trace. Solid (dashed) black line is the magnitude (phase) of the transform. Dotted gray line is the noise floor.

Temperature Dependence of the Absorption Spectrum

In Figure S2a, the UV-vis absorption spectrum of the NRL monolayer WS₂ sample is shown at several temperatures ranging from 295 to 20 K. To collect this data, we used a balanced deuterium tungsten source from Ocean Optics as our white light source and an Ocean Optics Jaz spectrometer module to measure the absorption spectrum. The white light was focused onto the NRL sample using gold off-axis parabolic (OAP) mirrors from within the terahertz setup. Since gold OAP mirrors have poor reflectivity in the visible, we were only able to measure the A exciton. To quantitatively track how the A exciton and the trion change with temperature, we modeled the absorption spectrum as a double Lorentzian. From the multi-peak fitting, we found that the A exciton peak shifts from 600 to 551 nm and that the trion absorption peak shifts from 614 to 563 nm (Figure S2b) as temperature is lowered from 295 to 20 K. To understand this blue shift of the absorption spectrum, we consider the fact that as the temperature is lowered, the band gap of the material increases.² Since the band gap is equal to the energy of the exciton plus the exciton binding energy, which does not have a strong temperature dependence, the energy of the exciton then must increase (blue shift) as the temperature is lowered. This effect has previously been observed in monolayer WS₂,³ as well as in other monolayer TMDs.⁴

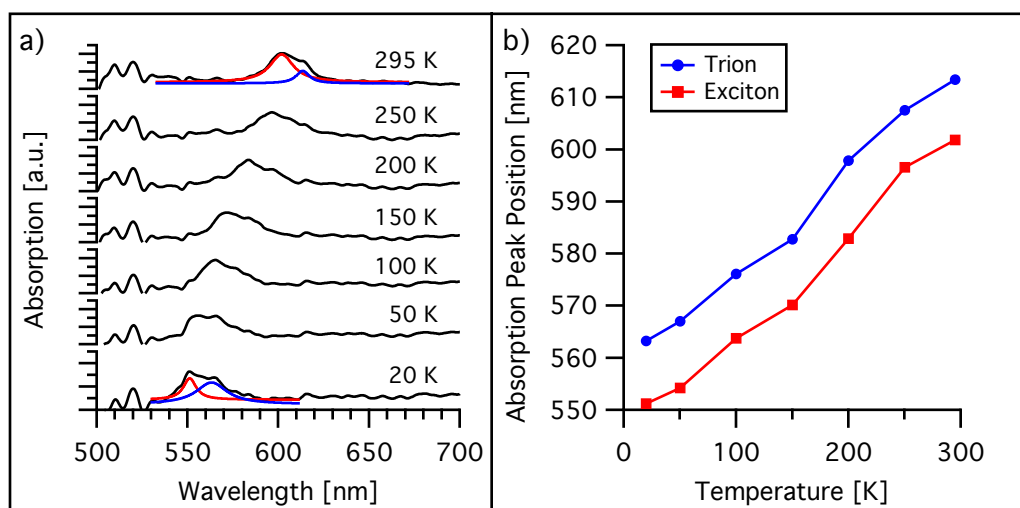


Figure S2. (a) Absorption spectrum (solid black lines) of the NRL monolayer WS₂ sample at several temperatures. Red (blue) lines at 295 and 20 K are the individual exciton (trion) peaks extracted from the multi-peak fitting. As the temperature decreases, the exciton line width narrows and the trion line width broadens. (b) Trion (blue circles) and exciton (red squares) absorption peak positions as a function of temperature.

In the commercial sample, we took the location of the A exciton at 20 K to be 584 nm⁵ as we did not have the capability to do a temperature-dependent absorption study on this sample.

Extraction of Conductivity

In order to determine the frequency-dependent photoconductivity of monolayer WS₂, we measured the entire pump-induced change in the transmitted terahertz field $\Delta E(t)$, as well as the entire transmitted terahertz field $E_0(t)$ through the sample when not excited. Then, after Fourier transforming the data and applying the thin-film approximation,⁶ we extracted the sheet photoconductivity using,

$$\Delta\tilde{\sigma}(\omega) = -\left(\frac{n+1}{Z_0}\right)\frac{\Delta\tilde{E}(\omega)}{\tilde{E}_0(\omega)} \quad (\text{S1})$$

where $n = 1.52$ is the refractive index of the TOPAS substrate and $Z_0 = 377 \Omega$ is the impedance of free space. From the relation above, we see that a transient decrease in the transmitted terahertz field ($\Delta E(t) < 0$) results in an increase in photoconductivity. In Figure S3a, we show a typical $\Delta E(t)$ and $E_0(t)$ waveform for monolayer WS₂, with corresponding spectra in S3b. Since the pump-induced change in the terahertz field $\Delta E(t)$ was extremely small (about 5000 times smaller than the reference $E_0(t)$), long averaging times were necessary in order to resolve the photoconductivity with sufficient signal-to-noise.

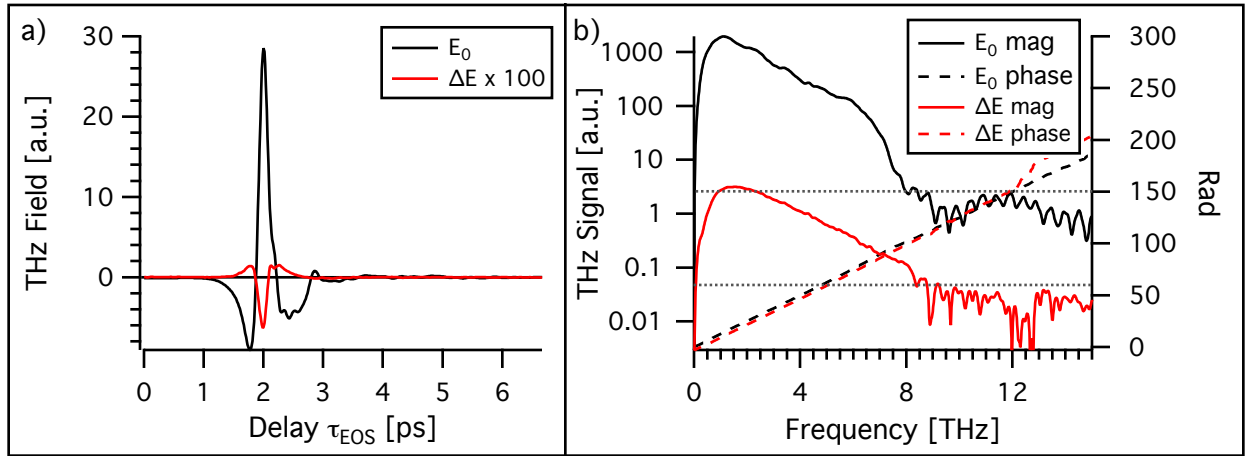


Figure S3. (a) Typical transmitted reference $E_0(t)$ (black line) and photo-modulated $\Delta E(t)$ (red line) terahertz waveforms for monolayer WS₂. (b) Fourier transforms of $E_0(t)$ and $\Delta E(t)$. Solid (dashed) black line is the magnitude (phase) of the $E_0(t)$ Fourier transform. Solid (dashed) red line is the magnitude (phase) of the $\Delta E(t)$ Fourier transform. Dotted gray lines are the noise floors for the respective spectra.

Positive Photoconductivity

The evidence and analysis presented in the main paper suggest that the source of positive photoconductivity in monolayer WS₂ is due to trions. Lui et al. on the other hand, report that trions in monolayer MoS₂ result in a negative photoconductivity.⁷ To address these differences, we mention that the monolayer MoS₂ sample studied by Lui et al. was n-doped. Being an n-doped material, the monolayer MoS₂ sample already had positive conductivity. Therefore, upon photoexcitation, the photoconductivity lowered because photogenerated electron hole pairs combined with the excess electrons in the MoS₂ to form trions, which have increased effective mass and thus lower conductivity. Since our sample is not doped, we observe a positive change in the photoconductivity. In our study, charge carriers only exist after photoexcitation and thus, there has to be a positive change in the conductivity. This assignment is verified by directly comparing, under the same experimental conditions, the rise in conductivity seen when exciting GaAs, a known Drude material with positive photoconductivity.

Calculation of Trion Mobility

To estimate the mobility of trions in monolayer WS₂ from the extracted fitting parameters presented in Tables 1 and 2, we looked at the first term of the three-oscillator model (Eq. 3), which is the Drude component. In the DC limit ($\omega = 0$), this Drude term reduces to

$$\Delta\sigma(\omega) = \frac{n_{\text{F}} e^2}{m \gamma_{\text{F}}} = n_{\text{F}} e \mu \quad (\text{S2})$$

where $\mu = e/m\gamma_{\text{F}}$ is the trion mobility. Using the extracted values of γ_{F} , we estimate the trion mobility to be roughly 60 cm²/ (V s) in the commercial sample and 900 cm²/ (V s) in the NRL sample. These results are higher than expected. Trion mobilities should be three times smaller than electron mobilities in monolayer WS₂, which are on the order of hundreds of cm²/ (V s). In monolayer WS₂, Jo et al.⁸ observes room temperature electron mobilities up to approximately 50 cm²/ (V s) and Ovchinnikov et al.⁹ observes electron mobilities as high as 140 cm²/ (V s). However, Zhang et al.¹⁰ predicts electron mobilities to be over 1000 cm²/ (V s) in monolayer WS₂. To understand these various results, we consider the fact that we make measurements at terahertz frequencies. At terahertz frequencies, we sample length scales on the order of tens of nanometers. At such a scale, we expect good crystalline order and thus higher mobilities.

To account for the difference in mobility between the commercial and NRL sample, we consider grain boundaries. Larger grain sizes in the NRL sample would suggest higher crystalline order on average and thus higher carrier mobilities. One piece of evidence that suggests that grain sizes are larger in the NRL sample is the smaller broad resonance frequency in the NRL sample than in the commercial sample. In the NRL sample, the broad resonance frequency is 3.2 THz (Table 2) and in the commercial sample, the broad resonance frequency is 4.4 THz (Table 1). In larger grain sizes, we expect a smaller broad resonance frequency since less charge builds up at the boundary.

Results from Above Resonance Pump Excitation

In addition to the on-resonance work presented in the main paper, we also investigated pumping monolayer WS₂ above the band gap. In Figure S4, we present the frequency-dependent photoconductivity of monolayer WS₂ (NRL film) pumped at 400 nm. Here, we find that the photoconductivity behaves the same as when the sample is pumped on resonance with the A exciton. This suggests that the initial free charge population achieved by pumping above gap cools down within hundreds of femtoseconds to form trions. Lui et al. observe a similar ultrafast trion formation time in monolayer MoS₂ with above-gap photoexcitation.⁷

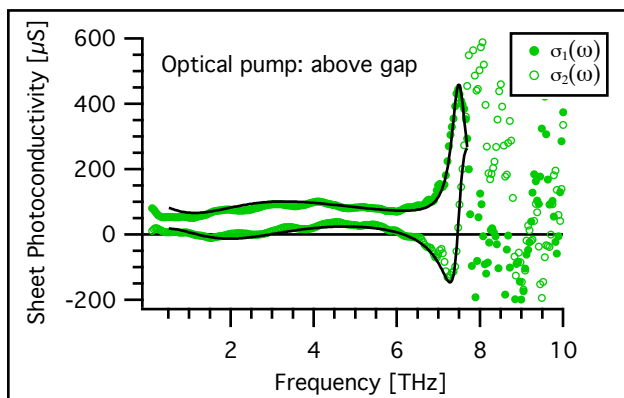


Figure S4. Complex frequency-dependent photoconductivity of monolayer WS₂ (NRL film) pumped above gap at 20 K (400 nm). Absorbed fluence was $\sim 5.6 \times 10^{13}$ photons/cm². Conductivity was probed 400 fs after excitation. Solid (open) circles are the real (imaginary) part of the induced photoconductivity. Solid lines represent fits to Eq. 2.

Note that the trion resonance measured while pumping above gap (Figure S4) is smaller in magnitude than the trion resonance measured while pumping on resonance with the A exciton (top plot in Figure 3) even though the conductivity was probed at the same time and the absorbed fluence was approximately the same. This suggests that trion formation is more efficient when pumping on resonance than when pumping above the gap. To understand this, we consider what happens when pumping above gap. During above gap photoexcitation, some of the absorbed photons generate free electron-hole pairs and some of the absorbed photons just create free holes by promoting electrons deep within the valence to immobile defect states. We therefore expect an increased dielectric screening environment (since we have a sea of electrons in the conduction band and a sea of holes in the valence band). This increased screening environment then weakens Coulombic interactions between electrons and holes and consequently reduces trion formation. A slight increase in the Drude component of the photoconductivity when pumping above gap further supports this argument since free electrons/holes have higher mobilities and thus contribute more to the low frequency conductivity.

References

1. Planken, P. C. M.; Nienhuys, H. K.; Bakker, H. J.; Wenckebach, T., Measurement and Calculation of the Orientation Dependence of Terahertz Pulse Detection in ZnTe. *J. Opt. Soc. Am. B* **2001**, *18*, 313-317.
2. O'Donnell, K. P.; Chen, X., Temperature Dependence of Semiconductor Band Gaps. *Appl. Phys. Lett.* **1991**, *58*, 2924-2926.
3. Plechinger, G.; Nagler, P.; Kraus, J.; Paradiso, N.; Strunk, C.; Schuller, C.; Korn, T., Identification of Excitons, Trions and Biexcitons in Single-Layer WS₂. *Phys. Status Solidi RRL* **2015**, *9*, 457-461.
4. Ross, J. S.; Wu, S. F.; Yu, H. Y.; Ghimire, N. J.; Jones, A. M.; Aivazian, G.; Yan, J. Q.; Mandrus, D. G.; Xiao, D.; Yao, W.; Xu, X. D., Electrical Control of Neutral and Charged Excitons in a Monolayer Semiconductor. *Nat. Commun.* **2013**, *4*, 1474.
5. Zhu, B. R.; Chen, X.; Cui, X. D., Exciton Binding Energy of Monolayer WS₂. *Sci. Rep.* **2015**, *5*, 9218.
6. Nienhuys, H. K.; Sundstrom, V., Intrinsic Complications in the Analysis of Optical-Pump, Terahertz Probe Experiments. *Phys. Rev. B: Condens. Matter Mater. Phys.* **2005**, *71*, 235110.
7. Lui, C. H.; Frenzel, A. J.; Pilon, D. V.; Lee, Y. H.; Ling, X.; Akselrod, G. M.; Kong, J.; Gedik, N., Trion-Induced Negative Photoconductivity in Monolayer MoS₂. *Phys. Rev. Lett.* **2014**, *113*, 166801.
8. Jo, S.; Ubrig, N.; Berger, H.; Kuzmenko, A. B.; Morpurgo, A. F., Mono- and Bilayer WS₂ Light-Emitting Transistors. *Nano Lett.* **2014**, *14*, 2019-2025.
9. Ovchinnikov, D.; Allain, A.; Huang, Y. S.; Dumcenco, D.; Kis, A., Electrical Transport Properties of Single-Layer WS₂. *ACS Nano* **2014**, *8*, 8174-8181.
10. Zhang, W. X.; Huang, Z. S.; Zhang, W. L.; Li, Y. R., Two-Dimensional Semiconductors with Possible High Room Temperature Mobility. *Nano Res.* **2014**, *7*, 1731-1737.